Icarus 212 (2011) 629–642

Contents lists available at ScienceDirect

Icarus

journal homepage: www.elsevier.com/locate/icarus

Modeling hot spring chemistries with applications to martian silica formation

G.M. Marion [a,*], D.C. Catling [b], J.K. Crowley [c], J.S. Kargel [d]

[a] Desert Research Institute, 2215 Raggio Parkway, Reno, NV 89512, USA
[b] University of Washington, Dept. Earth & Space Sciences, Seattle, WA 98195, USA
[c] United States Geological Survey, 12201 Sunrise Valley Dr., Reston, VA 20192, USA
[d] University of Arizona, Dept. Hydrology & Water Resources, Tucson, AZ 85721, USA

ARTICLE INFO

Article history:
Received 20 October 2010
Revised 26 January 2011
Accepted 27 January 2011

Keywords:
Mars, Surface
Geological processes
Mineralogy

ABSTRACT

Many recent studies have implicated hydrothermal systems as the origin of martian minerals across a wide range of martian sites. Particular support for hydrothermal systems include silica (SiO_2) deposits, in some cases >90% silica, in the Gusev Crater region, especially in the Columbia Hills and at Home Plate. We have developed a model called CHEMCHAU that can be used up to 100 °C to simulate hot springs associated with hydrothermal systems. The model was partially derived from FREZCHEM, which is a colder temperature model parameterized for broad ranges of temperature (<−70 to 25 °C), pressure (1–1000 bars), and chemical composition. We demonstrate the validity of Pitzer parameters, volumetric parameters, and equilibrium constants in the CHEMCHAU model for the Na–K–Mg–Ca–H–Cl–ClO_4–SO_4–OH–HCO_3–CO_3–CO_2–O_2–CH_4–Si–H_2O system up to 100 °C and apply the model to hot springs and silica deposits.

A theoretical simulation of silica and calcite equilibrium shows how calcite is least soluble with high pH and high temperatures, while silica behaves oppositely. Such influences imply that differences in temperature and pH on Mars could lead to very distinct mineral assemblages. Using measured solution chemistries of Yellowstone hot springs and Icelandic hot springs, we simulate salts formed during the evaporation of two low pH cases (high and low temperatures) and a high temperature, alkaline (high pH) sodic water. Simulation of an acid-sulfate case leads to precipitation of Fe and Al minerals along with silica. Consistency with martian mineral assemblages suggests that hot, acidic sulfate solutions are plausibility progenitors of minerals in the past on Mars. In the alkaline pH (8.45) simulation, formation of silica at high temperatures (355 K) led to precipitation of anhydrous minerals ($CaSO_4$, Na_2SO_4) that was also the case for the high temperature (353 K) low pH case where anhydrous minerals (NaCl, $CaSO_4$) also precipitated. Thus we predict that secondary minerals associated with massive silica deposits are plausible indicators on Mars of precipitation environments and aqueous chemistry. Theoretical model calculations are in reasonable agreement with independent experimental silica concentrations, which strengthens the validity of the new CHEMCHAU model.

1. Introduction

There are many studies recently that have implicated hydrothermal systems as drivers for martian geochemistries across a wide range of martian sites including hot spring deposits in Arabia Terra (Oehler and Allen, 2008); hydrated silica and ferric sulfates in Juventae Chasma (Bishop et al., 2009); sulfates in martian meteorites (McCubbin et al., 2008); hematite in Meridiani Planum (Golden et al., 2008); silica in Valles Marineris (Milliken et al., 2008); and silica-rich deposits in Gusev Crater (Squyres et al., 2007; Crumpler et al., 2008; Ming et al., 2008; Morris et al., 2008; Rice et al., 2008; Ruff et al., 2008; Yen et al., 2008). While most of these studies attribute these hydrothermal processes to magmatic fluids interacting with ground water or ice, there is also support for impact generated hydrothermal systems that can persist for 10^4 to $>10^5$ years (Schwenzer and Kring, 2008). Also of interest are possible geo/hydrothermal systems that are operative even for hundreds of millions or billions of years, without magmatic or other anomalous heat flow conditions, if high crustal temperatures are sustained by thick insulating deposits, such as hydrate materials (Kargel et al., 2007).

One of the leading empirical supports for hydrothermal systems are the massive silica (SiO_2) deposits, in some cases >90% silica, in the Gusev Crater region, especially in the Columbia Hills and at Home Plate (Crumpler et al., 2008; Ming et al., 2008; Morris et al., 2008; Rice et al., 2008; Ruff et al., 2008; Yen et al., 2008). On Earth, opaline silica is a common feature of hydrothermal springs (Rodgers et al., 2002), which is why the presence of such deposits on Mars suggests hydrothermal springs (Ruff et al.,

* Corresponding author. Fax: +1 775 673 7485.
E-mail address: Giles.Marion@dri.edu (G.M. Marion).

0019-1035/$ - see front matter © 2011 Elsevier Inc. All rights reserved.
doi:10.1016/j.icarus.2011.01.035

2008). While the preponderance of support is for hydrothermal formation of these high silica deposits, there is also an alternative hypothesis for weathering and diagenesis of olivine-bearing rocks (Tosca et al., 2004; Clark et al., 2005; McLennan et al., 2005; Glotch et al., 2006; McAdam et al., 2008). But in this paper dealing primarily with high temperatures, we will focus on hydrothermal formation of high silica deposits. And while some have argued for both past and present hydrothermal areas on Mars (Schulze-Makuch et al., 2007), the Mars Odyssey THEMIS analysis have found no evidence for endogenic heat sources on Mars (Christensen et al., 2003). However, given the widespread occurrence of volcanic features and impact craters, both magmatic and impact generated heat have been important at many intervals pretty much across the surface of Mars.

Previously we have explored the geochemical evolution of, and possible habitats for life on, Mars by developing a unique aqueous geochemical model (FREZCHEM) parameterized for broad ranges of temperatures (<−70 to 25 °C), pressure (1–1000 bars), and chemical composition. However, FREZCHEM cannot simulate hot springs because the upper temperature limit is 25 °C.

In this paper we (1) extend the validity of a FREZCHEM-like model to 100 °C for hot spring simulations (called CHEMCHAU), and (2) apply the model to hot spring environments, especially where there are massive silica deposits.

2. Methods and materials

2.1. FREZCHEM model

FREZCHEM is an equilibrium chemical thermodynamic model parameterized for concentrated electrolyte solutions (to ionic strengths ⩽20 m) using the Pitzer approach (Pitzer, 1991, 1995) for the temperature range from <−70 to 25 °C and the pressure range from 1 to 1000 bars (Marion and Farren, 1999; Marion, 2001, 2002; Marion et al., 2003a, 2005, 2006, 2008; Marion et al., 2009a,b, 2010a–c; Marion and Kargel, 2008). The current version of the model is parameterized for the Na–K–Mg–Ca–Fe(II)–Fe(III)–Al–H–Cl–ClO_4–Br–SO_4–NO_3–OH–HCO_3–CO_3–CO_2–O_2–CH_4–Si–H_2O system and includes 101 solid phases including ice, 15 chloride minerals, 35 sulfate minerals, 15 carbonate minerals, five solid-phase acids, three nitrate minerals, six perchlorates, six acid-salts, five iron oxide/hydroxides, four aluminum hydroxides, two silica minerals, two gas hydrates, and two bromide sinks (see above references for these model parameters).

2.2. Pitzer approach

In the Pitzer approach, the activity coefficients (γ) as a function of temperature at 1.01 bar pressure for cations (M), anions (X), and neutral aqueous species (N), such as CO_2(aq) or CH_4(aq), are given by

$$\ln(\gamma_M) = z_M^2 F + \sum m_a(2B_{Ma} + ZC_{Ma}) + \sum m_c(2\Phi_{Mc} + \sum m_a \Psi_{Mca}) + \sum\sum m_a m_{a'} \Psi_{Maa'} + z_M \sum\sum m_c m_a C_{ca} + 2\sum m_n \lambda_{nM} + \sum\sum m_n m_a \zeta_{nMa} \quad (1)$$

$$\ln(\gamma_X) = z_X^2 F + \sum m_c(2B_{cX} + ZC_{cX}) + \sum m_a(2\Phi_{Xa} + \sum m_c \Psi_{cXa}) + \sum\sum m_c m_{c'} \Psi_{cc'X} + |z_X| \sum\sum m_c m_a C_{ca} + 2\sum m_n \lambda_{nX} + \sum\sum m_n m_a \zeta_{ncX} \quad (2)$$

$$\ln(\gamma_N) = \sum m_c(2\lambda_{Nc}) + \sum m_a(2\lambda_{Na}) + \sum\sum m_c m_a \zeta_{Nca} \quad (3)$$

where B, C, Φ, Ψ, λ and ζ are Pitzer-equation interaction parameters, m_i is the molal concentration, and F and Z are equation functions. In these equations, the Pitzer interaction parameters and the F function are temperature dependent. The subscripts c, a, and n refer to cations, anions, and neutral species, respectively. C' and a' refer to cations and anions, respectively, that differ from c and a. The activity of water (a_w) at 1.01 bar pressure is given by

$$a_w = \exp\left(-\frac{\phi \sum m_i}{55.50844}\right) \quad (4)$$

where ϕ is the osmotic coefficient, which is given by

$$(\phi - 1) = \frac{2}{\sum m_i}\left\{\frac{-A_\phi I^{3/2}}{1 + bI^{1/2}} + \sum\sum m_c m_a \left(B_{ca}^{\phi} + ZC_{ca}\right) + \sum\sum m_c m_{c'}\left(\Phi_{cc'}^{\phi} + \sum m_a \Psi_{cc'a}\right) + \sum\sum m_a m_{a'}\left(\Phi_{aa'} + \sum m_c \Psi_{caa'}\right) + \sum\sum m_n m_c \lambda_{nc} + \sum\sum m_n m_a \lambda_{na} + \sum\sum\sum m_n m_c m_a \zeta_{n,c,a}\right\} \quad (5)$$

The binary B parameters in Eqs. (1), (2), and (5), are functions of $B_{ca}^{(0)}$, $B_{ca}^{(1)}$ and $B_{ca}^{(2)}$; similarly, the C parameters in these equations are a function of C_{ca}^{ϕ}.

FREZCHEM specifies the density and pressure dependence of equilibrium constants (K), activity coefficients (γ), and the activity of water (a_w). An example is how density is calculated with the equation

$$\rho = \frac{1000 + \sum m_i M_i}{\frac{1000}{\rho^0} + \sum m_i \overline{V}_i^0 + V_{mix}^{ex}} \quad (6)$$

where m_i is the molal concentration, M_i is the molar mass, ρ^0 is the density of pure water at a given temperature and pressure, $\overline{V}_i^0$ is the partial molar volume at infinite dilution of solution species, and V_{mix}^{ex} is the excess volume of mixing given by

$$V_{mix}^{ex} = A_v\left(\frac{I}{b}\right)\ln(1 + bI^{0.5}) + 2RT \times \sum\sum m_c m_a\left[B_{c,a}^{V} + \left(\sum m_c z_c\right)C_{c,a}^{v}\right] \quad (7)$$

where A_v is the volumetric Pitzer–Debye–Hückel parameter, I is the ionic strength, b is a constant (1.2 $kg^{0.5}$ $mol^{-0.5}$), and $B_{c,a}^{v}$ and $C_{c,a}^{v}$ are functions of $B_{ca}^{(0)V}$, $B_{ca}^{(1)V}$, $B_{ca}^{(2)V}$ and C_{ca}^{V}. See Marion et al. (2005), Marion and Kargel (2008), or Marion et al. (2008) for a complete description of these temperature–pressure equations.

The temperature and pressure dependencies of Pitzer parameters (discussed above) and solubility products (discussed below) are defined by the equation

$$P = a_1 + a_2 T + a_3 T^2 + a_4 T^3 + a_5/T + a_6 \ln(T) \quad (8)$$

where P is the Pitzer parameter or $\ln(K_{sp})$ and T is absolute temperature (K); exceptions to this equation are footnoted in tables.

2.3. CHEMCHAU model

We call the new hot spring model, which is built on the FREZCHEM foundation, CHEMCHAU (CHEMistry CHAUd, where chaud means "hot" in French). This model is for the Na–K–Mg–Ca–H–Cl–ClO_4–SO_4–OH–HCO_3–CO_3–CO_2–O_2–CH_4–Si–H_2O chemical system. We extended the FREZCHEM model from an upper temperature range of 25 °C to 100 °C for CHEMCHAU. The chloride and carbonate chemistries within FREZCHEM were based in part on temperatures to 90 °C (Spencer et al., 1990; He and Morse, 1993). So these chemistries were easy to develop for CHEMCHAU. Extending perchlorate, sulfate, and silicon chemistries largely relied on existing models that included these chemistries in many cases to

temperatures >100 °C (Moller, 1988; Greenberg and Moller, 1989; Millero and Pierrot, 1998). But to maintain an accurate model, it was necessary in many cases to re-estimate the equilibrium constants and some Pitzer parameters. Several examples will be discussed in the Results. The CHEMCHAU model (Fortran code) will be released to interested scientists in the near future at http://frezchem.dri.edu.

3. Results

3.1. Pitzer parameterization and solubility products

In this section, we will present tables and figures that contain new equations that are components of CHEMCHAU. Excluded from these tables and figures are old equations from FREZCHEM that carried over into CHEMCHAU (e.g., binary equations for NaCl). See Marion and Kargel (2008) for a listing of these older equations. The structure of this revised model has parameters from FREZCHEM to cope with lower temperatures (⩽25 °C); but as temperature ranges exceed FREZCHEM, the program selects new temperature parameters from CHEMCHAU. Examples are discussed below.

The original version of FREZCHEM contained many Pitzer parameters from Spencer et al. (1990), which, in turn, were based on earlier references (e.g., Moller, 1988; Greenberg and Moller, 1989) that were programmed for higher temperatures (100 °C) than the FREZCHEM model (25 °C). As a consequence, many of the original Pitzer parameters in FREZCHEM easily extended to 90–100 °C. For example, NaCl, KCl, and $MgCl_2$ Pitzer parameters in CHEMCHAU are the same as in FREZCHEM. The only differences in model parameterizations for these three chloride chemistries were the equilibrium constants that had to include higher temperatures (Fig. 1, Table 1). A chloride exception to this general rule deals with $CaCl_2$, where we used Pitzer parameters from Millero and Pierrot (1998) that covered the temperature range from 0 to 100 °C (Table 2). While we included $CaCl_2$ Pitzer parameters in CHEMCHAU, we excluded $CaCl_2$ minerals because these minerals have a solubility of 14.33 m (I = 43.0 m) at 100 °C (Linke, 1958), which is beyond the ionic strength range of FREZCHEM/CHEMCHAU ($I \approx 20$ m). Moreover, $CaCl_2$ minerals are rare on Earth (Marion, 1997) and likely even more rare on Mars (Marion et al., 2009a).

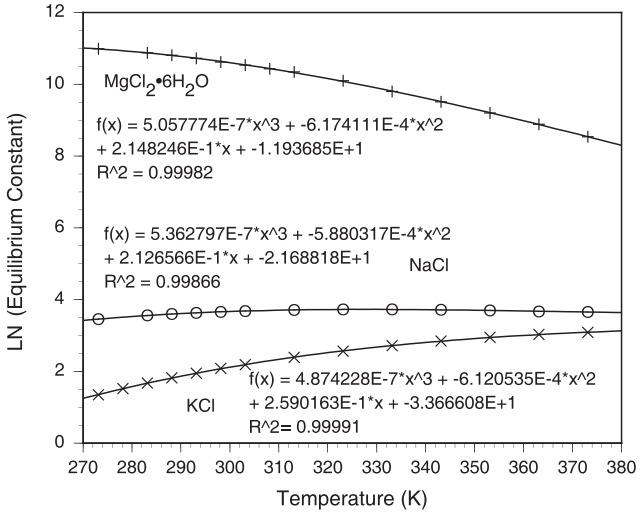

Fig. 1. The natural logarithms of the equilibrium constants for halite (NaCl), sylvite (KCl), and bischofite ($MgCl_2{\cdot}6H_2O$) over the 273–373 K temperature range (data from Linke (1965)).

The original incorporation of bicarbonate and carbonate chemistries (Na, K, Mg, and Ca) into FREZCHEM (Marion, 2001) was based on the He and Morse (1993) study where their temperature range was 0–90 °C. So for the most part, these chemistries did not need to be re-examined for CHEMCHAU. But it was necessary to re-evaluate the bicarbonate–carbonate equilibrium constants to extend the temperature range to 100 °C. Fig. 2 is an example for Na_2CO_3 minerals; Table 1 includes all the new Na–K–Mg bicarbonate–carbonate equilibrium constants.

While chloride, bicarbonate, and carbonate Pitzer parameters from FREZCHEM worked well for CHEMCHAU, this was not the case for sulfate and perchlorate chemistries. Sulfate Pitzer parameters for K_2SO_4 and $MgSO_4$ were taken from Millero and Pierrot (1998) that covered the temperature range from 0 to 100 °C (Table 2). It was necessary to add new equilibrium constants for these chemistries at higher temperatures (Fig. 3, Table 1). The Na_2SO_4 Pitzer parameters were taken from Moller (1988) that covered the temperature range from 25 to 250 °C; given these parameters, the model developed excellent fits to equilibrium data (Linke, 1965) that covered the 0–100 °C temperature range (Fig. 4, Table 1). Neither of these two sulfate references (Moller, 1988; Millero and Pierrot, 1998) fit the existing FREZCHEM $CaSO_4$ data well. In CHEMCHAU, we used FREZCHEM values for $CaSO_4$ Pitzer parameters and the equilibrium constant for $CaSO_4{\cdot}2H_2O$ (gypsum). In addition, we added $CaSO_4$ (anhydrite) to the model based on the experimental data used by Moller (1988). The subsequent peritectic for $CaSO_4$–$CaSO_4{\cdot}2H_2O$ was estimated at 52 °C, which is in the range for this poorly defined peritectic (40–60 °C) (Raju and Atkinson, 1990).

New Pitzer parameters for Na–Mg–Ca perchlorates were taken from Millero and Pierrot (1998) (Table 2). We used the FREZCHEM Pitzer parameters for the insoluble $KClO_4$ (Marion et al., 2010a). Equilibrium constants for perchlorate salts are summarized in Table 1. Fig. 5 is a perchlorate example depicting $NaClO_4$ equilibrium constants. As was the case for $CaCl_2$, we also eliminated $Ca(ClO_4)_2$ from our mineral database because this mineral approaches an ionic strength of 64 m at 93 °C, which is beyond the validity of this model ($I \approx 20$ m). As we pointed out for $CaCl_2$, $Ca(ClO_4)_2$ is also likely rare on Earth and Mars (Marion et al., 2010a).

One of the major reasons for developing the hot spring model was to deal with SiO_2 chemistries on Mars where massive SiO_2 deposits are believed due to hydrothermal activity in the Home Plate region of Gusev Crater (Morris et al., 2008; Ruff et al., 2008; Squyres et al., 2008). CHEMCHAU includes an equilibrium constant for SiO_2(amorphous) that covers the temperature range from 273 to 373 K (Table 1). We also included equations that cover binaries between cation(or anion) and the neutral SiO_2 (Table 3). These equations cover the temperature range from 25 to 300 °C. We placed these binaries in a separate table from Table 2 because the temperature equations are very different, and the binary symbols ($B^{(0)}_{i,j}$ vs. $\lambda_{i,Si_{O_2}}$) are also different between cation–anion and cation(or anion)-neutral species associations.

In Table 4 are ternary Pitzer parameters from Millero and Pierrot (1998) that extend the temperature scale to ranges beyond 25 °C. Scattered in Tables 1 and 2 are a few other equilibrium constants and Pitzer parameters that were necessary to extend to higher temperatures, especially $K_w = (H^+)(OH^-)/(H_2O)$ in Table 1. Also hypercritical is the Debye–Hückel model parameter (A_ϕ) that is a component in both Eqs. (1) and (2) (within the "F" term) and Eq. (5). This equation used in CHEMCHAU is

$$\begin{aligned} A_\phi = {} & 3.36901532e-1 - 6.32100430e-4 * T \\ & + 9.14252359/T - 1.35143986e-2 * \ln(T) \\ & + 2.26089488e-3/(T-263) + 1.92118597e-6 * T^2 \\ & + 4.52586464e1/(680-T) \end{aligned} \quad (9)$$

Table 1
Ln(Equilibrium constants) added to the CHEMCHAU model.

	a_1	a_2	a_3	a_4	Temperature range (K)	References
Solution–solid phase equilibria						
$NaCl(cr) \Longleftrightarrow Na^+(aq) + Cl^-(aq)$	−2.168818e1	2.126566e−1	−5.880317e−4	5.362797e−7	273–373	Linke (1965) and this work
$KCl(cr) \Longleftrightarrow K^+(aq) + Cl^-(aq)$	−3.366608e1	2.590163e−1	−6.120535e−4	4.874228e−7	273–373	Linke (1965) and this work
$Mg(Cl)_2 \cdot 6H_2O(cr) \Longleftrightarrow Mg^{2+}(aq) + 2Cl^-(aq) + 6H_2O(l)$	−1.193685e1	2.148246e−1	−6.174111e−4	5.057774e−7	273–373	Linke (1965) and this work
$NaClO_4(cr) \Longleftrightarrow Na^+(aq) + ClO_4^-(aq)$	4.222898e1	−2.259533e−1	3.581663e−4		324–373	Linke (1965) and this work
$NaClO_4 \cdot H_2O(cr) \Longleftrightarrow Na^+(aq) + ClO_4^-(aq) + H_2O(l)$	3.423186e−2	1.669594e−2			273–324	Linke (1965) and this work
$KClO_4(cr) \Longleftrightarrow K^+(aq) + ClO_4^-(aq)$	−1.090074e1	−1.175019e−1	7.686483e−4	−1.017366e−6	273–373	Linke (1965) and this work
$Mg(ClO_4)_2 \cdot 6H_2O(cr) \Longleftrightarrow Mg^{2+}(aq) + 2ClO_4^-(aq) + 6H_2O(l)$	−1.264842e1	1.440957e−1	−1.944892e−4		273–366	Linke (1965), Dobrynina et al. (1980), Pestova et al. (2005) and this work
$Na_2SO_4(cr) \Longleftrightarrow 2Na^+(aq) + SO_4^{2-}(aq)$	1.396088e0	−2.075476e−3	−1.603548e−5		306–373	Linke (1965) and this work
$Na_2SO_4 \cdot 10H_2O(cr) \Longleftrightarrow 2Na^+(aq) + SO_4^{2-}(aq) + 10H_2O(l)$	−8.169880e1	4.215485e−1	−5.263219e−4		273–306	Linke (1965) and this work
$K_2SO_4(cr) \Longleftrightarrow 2K^+(aq) + SO_4^{2-}(aq)$	−5.220127e1	3.547613e−1	−8.501496e−4	6.746759e−7	273–373	Linke (1965) and this work
$MgSO_4 \cdot H_2O(cr) \Longleftrightarrow Mg^{2+}(aq) + SO_4^{2-}(aq) + H_2O(l)$	1.944901e1	−6.487989e−2			342–373	Linke (1965) and this work
$MgSO_4 \cdot 6H_2O(cr) \Longleftrightarrow Mg^{2+}(aq) + SO_4^{2-}(aq) + 6H_2O(l)$	−2.507900e1	1.342215e−1	−2.113096e−4		321–342	Linke (1965) and this work
$MgSO_4 \cdot 7H_2O(cr) \Longleftrightarrow Mg^{2+}(aq) + SO_4^{2-}(aq) + 7H_2O(l)$	−2.581461e1	1.266418e−1	−1.821663e−4		273–321	Linke (1965) and this work
$CaSO_4(cr) \Longleftrightarrow Ca^{2+}(aq) + SO_4^{2-}(aq)$	−1.193844e1	3.728778e−2	−1.025801e−4		325–373	Moller (1988) and this work
$NaHCO_3(cr) \Longleftrightarrow Na^+(aq) + HCO_3^-(aq)$	1.479309e1	−2.427724e−1	1.002818e−3	−1.224329e−6	273–373	Linke (1965) and this work
$Na_2CO_3 \cdot H_2O(cr) \Longleftrightarrow 2Na^+(aq) + CO_3^{2-}(aq) + H_2O(l)$	−6.625585e1	4.250286e−1	−6.681267e−4		309–373	Linke (1965) and this work
$Na_2CO_3 \cdot 7H_2O(cr) \Longleftrightarrow 2Na^+(aq) + CO_3^{2-}(aq) + 7H_2O(l)$	−2.358403e1	7.563798e−2			305–309	Linke (1965) and this work
$Na_2CO_3 \cdot 10H_2O(cr) \Longleftrightarrow 2Na^+(aq) + CO_3^{2-}(aq) + 10H_2O(l)$	−1.374373e1	−1.720902e−2	1.917331e−4		273–305	Linke (1965) and this work
$NaHCO_3 \cdot Na_2CO_3 \cdot 3H_2O(cr) \Longleftrightarrow 3Na^+(aq) + HCO_3^-(aq) + CO_3^{2-}(aq) + 3H_2O(l)$	−8.780646e1	5.044060e−1	−7.302884e−4		298–373	Linke (1965) and this work
$KHCO_3(cr) \Longleftrightarrow K^+(aq) + HCO_3^{2-}(aq)$	7.470347e0	−8.353955e−2	2.010238e−4		273–343	Linke (1965) and this work
$MgCO_3 \cdot 3H_2O \Longleftrightarrow Mg^{2+}(aq) + CO_3^{2-}(aq) + 3H_2O(l)$	−6.521206e0	−1.912580e−2			278–333	Linke (1965) and this work
$MgCO_3 \cdot 5H_2O \Longleftrightarrow Mg^{2+}(aq) + CO_3^{2-}(aq) + 5H_2O(l)$	6.196049e1	−5.297716e−1	9.492946e−4		271–293	Linke (1965) and this work
$SiO_2(amorphous) + 2H_2O(l) \Longleftrightarrow Si(OH)_4^0(aq)$	−4.397647e1	2.125224e−1	−2.896194e−4		273–373	Linke (1965) and this work
Solution-gas phase equilibria						
$HCl(g) \Longleftrightarrow HCl(aq)$	6.334279e1	−2.261957e−1	2.094907e−4		273–330	Carslaw et al. (1995)
$H_2O(l) \Longleftrightarrow H^+(aq) + OH^-(aq)$	−1.261242e2	6.724689e−1	−1.596758e−3	1.333644e−6	273–373	Greenberg and Moller (1989)
$H_2O(g) \Longleftrightarrow H_2O(l)$	5.783246e1	−3.601496e−1	7.810536e−4	−6.199883e−7	270–370	Lide (1994) and this work

which has been used by several Pitzer modeling groups (e.g., Moller, 1988; Greenberg and Moller, 1989; Millero and Pierrot, 1998) and covers the temperature range from 25 to 250 °C.

3.2. Density and pressure parameterizations

The FREZCHEM model is structured to predict density and the effects of pressure on chemical equilibria (Marion et al., 2005, 2008, 2009b, 2010a; Marion and Kargel, 2008). CHEMCHAU, on the other hand, is somewhat more limited with respect to density and pressure effects. Implementation of the density/pressure equations requires a specification of the partial molar volume $\left(V_i^0\right)$ and compressibility $\left(K_i^0\right)$ of individual species (e.g., Na^+, Mg^{2+}, SO_4^{2-}, ClO_4^-), binary Pitzer equation volumetric parameters ($B_{c,a}^{\nu}$, Table 2), and the density and molar volumes of water. Examples are Eqs. (6) and (7).

The equation that is used to estimate the density of pure water (ρ^0) (kg/m^3) or the molar volume of pure water ($1/\rho^0 = V^0$) as a function of temperature (K) and pressure (MPa) is given by

$$\begin{aligned}\rho^0 = {} & -856.361 + 20.4479 * T + 6.29682 * P - 4.7590e-2 \\ & * P * T - 8.2958e-2 * T^2 - 4.71347e-3 * P^2 \\ & + 2.73547e-5 * T * P^2 + 1.26422e-4 * P * T^2 \\ & + 1.48965e-4 * T^3 - \tilde{1}.61842\tilde{e}6P^3 - 1.03372e-7 \\ & * T^4 - 1.09178e-7 * P * T^3 - 4.41289e-8 * P^2 * T^2 \\ & + 6.94842e-9 * T * P^3 \end{aligned} \quad (10)$$

Table 2
Binary Pitzer-equation parameters for cations and anions derived for use in the CHEMCHAU model. Pitzer parameters not included in this table [Cl (Na, K, Mg), HCO_3 + CO_3 (Na, K, Mg, Ca), SO_4 (Ca), and ClO_4 (K)] are available from the FREZCHEM model (Marion and Kargel, 2008) and Marion et al. (2010a).

Pitzer parameters	a_1	a_2	a_3	a_4	a_5	a_6	Temperature range (K)	References
$B^{(0)}_{Ca,Cl}$	−9.794950e0	9.093629e−2	−2.716439e−4	2.692768e−7			273–373	Millero and Pierrot (1998)
$B^{(1)}_{Ca,Cl}$	3.478560e0	−1.541609e−2	3.178955e−5				273–373	Millero and Pierrot (1998)
$C^{\phi}_{Ca,Cl}$	1.025271e0	−8.889487e−3	2.586435e−5	−2.535034e−8			273–373	Millero and Pierrot (1998)
$B^{(0)}_{Na,ClO_4}$	−1.811927e−1	1.584621e−3	−2.655185e−6				273–348	Millero and Pierrot (1998) and this study
$B^{(1)}_{Na,ClO_4}$	−2.183392e0	1.646897e−2	−2.759549e−5				273–348	Millero and Pierrot (1998) and this study
C^{ϕ}_{Na,ClO_4}	2.058354e−2	−1.457641e−4	2.442399e−7				273–348	Millero and Pierrot (1998) and this study
$B^{(0)}_{Mg,ClO_4}$	3.4027e−1	5.2275e−4					273–366	Millero and Pierrot (1998) and this study
$B^{(1)}_{Mg,ClO_4}$	6.668e−1	4.50e−4					273–366	Millero and Pierrot (1998) and this study
C^{ϕ}_{Mg,ClO_4}	1.14727e−1	−3.5267e−4					273–366	Millero and Pierrot (1998) and this study
$B^{(0)}_{Ca,ClO_4}$	2.03810e−1	8.295e−4					273–323	Millero and Pierrot (1998)
$B^{(1)}_{Ca,ClO_4}$	2.426e−1	5.0775e−3					273–323	Millero and Pierrot (1998)
C^{ϕ}_{Ca,ClO_4}	8.7181e−2	−3.0918e−4					273–323	Millero and Pierrot (1998)
$B^{(0)}_{K,OH}$	−2.365594e−1	2.453709e−3	−4.111345e−6				273–323	Millero and Pierrot (1998)
$B^{(1)}_{K,OH}$	−6.830057e−1	6.717714e−3	−1.125603e−5				273–323	Millero and Pierrot (1998)
$C^{\phi}_{K,OH}$	2.880402e−2	−1.654597e−4	2.772439e−7				273–323	Millero and Pierrot (1998)
$B^{(0)}_{Na,HSO_4}$	5.890e0	−3.40104e−2	5.3937e−5				273–373	Millero and Pierrot (1998)
$B^{(1)}_{Na,HSO_4}$	5.87784e0	−1.8431e−2					273–373	Millero and Pierrot (1998)
C^{ϕ}_{Na,HSO_4}	3.905e−3						273–373	Millero and Pierrot (1998)
$B^{(0)}_{Na,SO_4}$	−2.705778e0	1.543350e−2	−2.121118e−5				298–373	Moller (1988)
$B^{(1)}_{Na,SO_4}$	−4.438919e0	3.086813e−2	−4.132221e−5				298–373	Moller (1988)
C^{ϕ}_{Na,SO_4}	4.777799e−1	−2.644687e−3	3.573726e−6				298–373	Moller (1988)
$B^{(0)}_{K,SO_4}$	4.07908797e1	8.26906675e−3			−1.41842998e3	−6.74728848e0	273–373	Millero and Pierrot (1998)
$B^{(1)}_{K,SO_4}$	−1.31669651e1	2.35793239e−2			2.06712594e3		273–373	Millero and Pierrot (1998)
C^{ϕ}_{K,SO_4}	−1.88e−2						273–373	Millero and Pierrot (1998)
$B^{(0)}_{Mg,SO_4}$	−3.656954e−1	3.114461e−3	−3.948514e−6				298–373	Millero and Pierrot (1998)
$B^{(1)}_{Mg,SO_4}$	−1.545900e0	2.167785e−2	−1.764903e−5				298–373	Millero and Pierrot (1998)
$B^{(2)}_{Mg,SO_4}$	−3.419500e2	2.292600e0	−4.205515e−3				298–373	Millero and Pierrot (1998)
C^{ϕ}_{Mg,SO_4}	1.940163e−1	−7.328694e−4	5.965184e−7				298–373	Millero and Pierrot, 1998
Volumetric parameters[a]								
$B^{v(0)}_{Na,Cl}$	1.2335e−5	−2.7445e−7	2.4624e−9	−1.08e−12			278–368	Krumgalz et al. (2000)
$B^{v(1)}_{Na,Cl}$	4.354e−6	−9.259e−7	2.980e−8	−3.27e−10			278–368	Krumgalz et al. (2000)
$C^{v}_{Na,Cl}$	−6.578e−7	1.5101e−8	−5.5e−12	−1.6e−13			278–368	Krumgalz et al. (2000)
$B^{v(0)}_{Na,SO_4}$	5.3250e−5	−1.0930e−6	5.5828e−8	−4.6248e−10			288–368	Krumgalz et al. (2000)
$B^{v(1)}_{Na,SO_4}$	1.2932e−4	−5.1406e−6	−1.3311e−7	1.552Ee−9			288–368	Krumgalz et al. (2000)
C^{v}_{Na,SO_4}	−2.9140e−6	1.0798e−7	−9.5282e−9	7.375e−11			288–368	Krumgalz et al. (2000)
$B^{v(0)}_{Na,HCO_3}$	−1.1620e−5	−2.8646e−6	−5.1284e−7				278–318	Krumgalz et al., 2000
$B^{v(1)}_{Na,HCO_3}$	1.7800e−4	4.4518e−6	1.3897e−6				278–318	Krumgalz et al. (2000)
C^{v}_{Na,HCO_3}	1.3741e−5	7.3175e−7	1.4971e−7				278–318	Krumgalz et al. (2000)
$B^{v(0)}_{Na,CO_3}$	5.9800e−5	−6.9018e−7	2.1120e−9				288–333	Krumgalz et al. (2000)
$B^{v(1)}_{Na,CO_3}$	8.1600e−5	−7.4232e−6	1.5774e−7				288–333	Krumgalz et al. (2000)
C^{v}_{Na,CO_3}	−3.2500e−6	1.6502e−8	6.157e−10				288–333	Krumgalz et al. (2000)
$B^{v(0)}_{K,Cl}$	1.2793e−5	−1.8784e−7	−1.2365e−9	−2.720e−11			288–368	Krumgalz et al. (2000)

(*continued on next page*)

Table 2 (*continued*)

Pitzer parameters	a_1	a_2	a_3	a_4	a_5	a_6	Temperature range (K)	References
$B^{v(1)}_{K,Cl}$	8.948e−6	−1.0948e−6	5.473e−8	−3.00e−10			288–368	Krumgalz et al. (2000)
$C^{v}_{K,Cl}$	−7.131e−7	6.042e−9	6.737e−10	−9.52e−12			288–368	Krumgalz et al. (2000)
$B^{v(0)}_{K,SO_4}$	1.1054e−5	8.2980e−6	−2.6393e−7	1.8459e−9			288–368	Krumgalz et al. (2000)
$B^{v(1)}_{K,SO_4}$	2.6016e−4	−2.8743e−5	7.6066e−7	−4.988e−9			288–368	Krumgalz et al., 2000
C^{v}_{K,SO_4}	1.6192e−5	−4.3294e−6	1.3595e−7	−1.0219e−9			288–368	Krumgalz et al. (2000)
$B^{v(0)}_{K,HCO_3}$	−7.241e−5						298	Krumgalz et al. (2000)
$B^{v(1)}_{K,HCO_3}$	2.4275e−4						298	Krumgalz et al. (2000)
C^{v}_{K,HCO_3}	3.9791e−5						298	Krumgalz et al. (2000)
$B^{v(0)}_{K,CO_3}$	3.4930e−5	−6.7348e−7	4.4902e−8	−9.3417e−10			293–333	Krumgalz et al. (2000)
$B^{v(1)}_{K,CO_3}$	1.6511e−4	−2.0346e−6	−8.2554e−7	2.0615e−8			293–333	Krumgalz et al., 2000
C^{v}_{K,CO_3}	−8.468e−7	2.4085e−8	−1.9939e−9	4.258e−11			293–333	Krumgalz et al. (2000)
$B^{v(0)}_{Mg,Cl}$	1.6933e−5	−4.605e−8	5.7990e−9	−7.328e−11			288–368	Krumgalz et al. (2000)
$B^{v(1)}_{Mg,Cl}$	−5.2068e−5	−6.3193e−6	−4.094e−8	1.001e−9			288–368	Krumgalz et al., 2000
$C^{v}_{Mg,Cl}$	−5.698e−7	−5.530e−9	−3.070e−10	4.74e−12			288–368	Krumgalz et al. (2000)
$B^{v(0)}_{Mg,SO_4}$	4.9809e−5	−4.2924e−7	3.413e−10				288–368	Krumgalz et al. (2000)
$B^{v(1)}_{Mg,SO_4}$	1.4491e−4	−8.3021e−6	5.385e−8				288–368	Krumgalz et al. (2000)
C^{v}_{Mg,SO_4}	3.969e−7	−2.3555e−8	2.738e−10				288–368	Krumgalz et al. (2000)
$B^{v(0)}_{Ca,Cl}$	1.3107e−5	−2.2290e−7	1.6253e−8	−4.3892e−10			288–328	Krumgalz et al., 2000
$B^{v(1)}_{Ca,Cl}$	−2.4575e−5	−8.388e−7	−1.7754e−7	5.152e−9			288–328	Krumgalz et al. (2000)
$C^{v}_{Ca,Cl}$	−1.265e−7	1.1014e−8	−8.674e−10	2.471e−11			288–328	Krumgalz et al. (2000)
$B^{v(0)}_{H,Cl}$ [b]	2.627667e−3	−8.216550e−6					333–373	ICT (1928) and this work
$B^{v(1)}_{H,Cl}$ [b]	−7.384914e−3	2.290882e−5					333–373	ICT (1928) and this work
$C^{v}_{H,Cl}$ [b]	−7.174925e−4	2.255337e−6					333–373	ICT (1928) and this work
$B^{v(0)}_{H,SO_4}$ [c]	1.299059e−2	−4.307449e−5					303–373	ICT (1928) and this work
$B^{v(1)}_{H,SO_4}$ [c]	−2.869194e−2	4.321832e−5	1.836706e−7				303–373	ICT (1928) and this work
C^{v}_{H,SO_4} [c]	−2.411227e−3	8.008289e−6					303–373	ICT (1928) and this work
$B^{v(0)}_{H,HSO_4}$ [c]	0.00						303–373	ICT (1928) and this work
$B^{v(1)}_{H,HSO_4}$ [c]	0.00						303–373	ICT (1928) and this work
C^{v}_{H,HSO_4} [c]	0.00						303–373	ICT (1928) and this work
$V^{(0)}_{H}$	0.00						273–373	Millero (1983)
$V^{(0)}_{Cl}$	−1.02412e2	7.8012e−1	−1.264e−3				273–323 (373)[d]	Millero (1983) and Marion and Kargel (2008)
$V^{(0)}_{Na}$	5.322068e1	−3.759538e−1	6.553571e−4				323–373	Linke (1965) and this work
$V^{(0)}_{K}$	−1.868106e2	1.132069e0	−1.622423e−3				323–373	Linke (1965) and this work
$V^{(0)}_{Mg}$	−4.964763e1	9.133945e−2					313–383	Linke (1965) and this work
$V^{(0)}_{Ca}$	8.759619e2	−8.218658e0	2.510729e−2	−2.546297e−5			323–373	ICT (1928) and this work
$V^{(0)}_{ClO_4}$	7.101897e1	−3.923986e−1	1.785629e−3	−2.567976e−6			273–373	Linke (1965) and this work
$V^{(0)}_{SO_4}$	−2.113165e2	1.278430e0	−1.758064e−3				303–375	Linke (1965) and this work
$V^{(0)}_{HCO_3}$	6.166538e3	−6.526572e1	2.323835e−1	−2.774642e−4			273–343	Linke (1965) and this work
$V^{(0)}_{CO_3}$	−4.048896e2	2.615278e0	−4.257950e−3				273–343	ICT (1928) and this work

[a] The equations for these volumetric binary parameters are: $f(T) = a_1 + a_2(T - 298.15) + a_3(T - 298.15)^2 + a_4(T - 298.15)^3$ except for the acid (HCl and H_2SO_4) parameters that are defined by Eq. (8).

[b] These equations are temperature supplements to similar equations in FREZCHEM (Marion and Kargel, 2008) and are to be used only for temperatures above 333.15 K.

[c] These equations are temperature supplements to similar equations in FREZCHEM (Marion and Kargel, 2008) and are to be used only for temperatures above 303.15 K.

[d] This equation was originally parameterized for the temperature range from 273 to 323 K (Millero, 1983). We assumed that this equation would work to 373 K, which was used to define volumetric parameters for Na, K, Mg, and Ca.

which covers the temperature range from 264 to 375 K, and the pressure range from 0.05 to 100 MPa (0.5–1000 bars). The data for this calculation were taken from Wagner and Pruss (2002). The standard error for this set of 551 data is 0.0226 kg/m^3 (22.6 ppm). Another volumetric parameter that is a major parameter for density/pressure calculations (Eq. (7)) is the volumetric Pitzer–Debye–Hückel parameter (A_v) (cm^3 kg$^{1/2}$ mol$^{-3/2}$) as a function of temperature (K) and pressure (bars) that is given by

$$\begin{aligned} A_v = {} & -7.02111 + 0.091808 * T - 6.35498e-3 * P \\ & + 4.71221e-5 * T * P - 3.72098e-4 * T^2 + 1.97050e \\ & - 6 * P^2 - 9.08153e-8 * T^2 * P - 1.41488e-8 * P^2 \\ & * T + 5.50669e-7 * T^3 + 2.58628e-11 * T^2 * P^2 \end{aligned} \quad (11)$$

which covers the temperature range from 273 to 373, and the pressure range from 1 to 1000 bars. The data for this calculation were

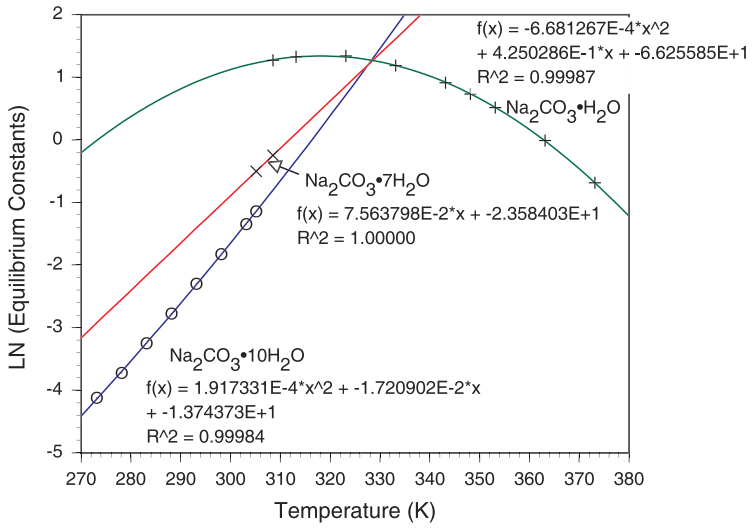

Fig. 2. The natural logarithms of the equilibrium constants for natron ($Na_2CO_3{\cdot}10H_2O$), ($Na_2CO_3{\cdot}7H_2O$), and thermonatrite ($Na_2CO_3{\cdot}H_2O$) over the 273–373 K temperature range (data from Linke (1965)).

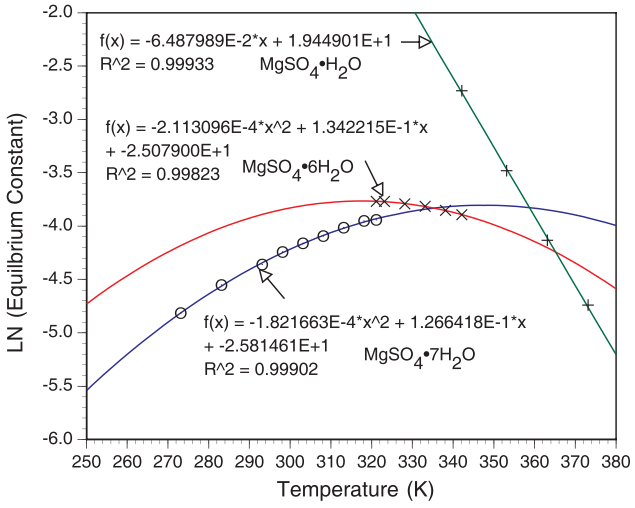

Fig. 3. The natural logarithms of the equilibrium constants for epsomite ($MgSO_4{\cdot}7H_2O$), hexahydrite ($MgSO_4{\cdot}6H_2O$), and kieserite ($MgSO_4{\cdot}H_2O$) over the 273–373 K temperature range (data from Linke (1965)).

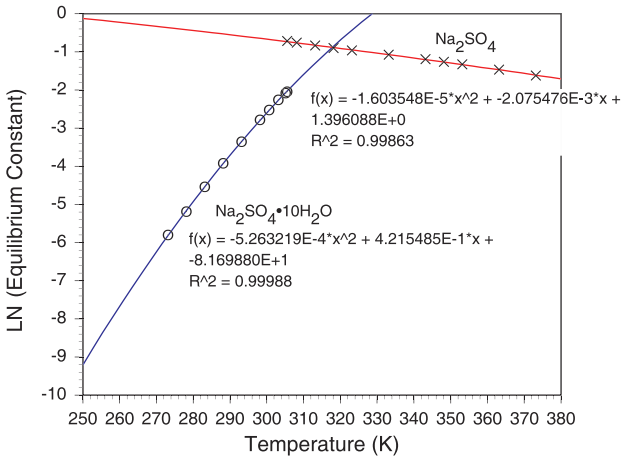

Fig. 4. The natural logarithms of the equilibrium constants for mirabilite ($Na_2SO_4{\cdot}10H_2O$) and thenardite (Na_2SO_4) over the 273–373 K temperature range (data from Linke (1965)).

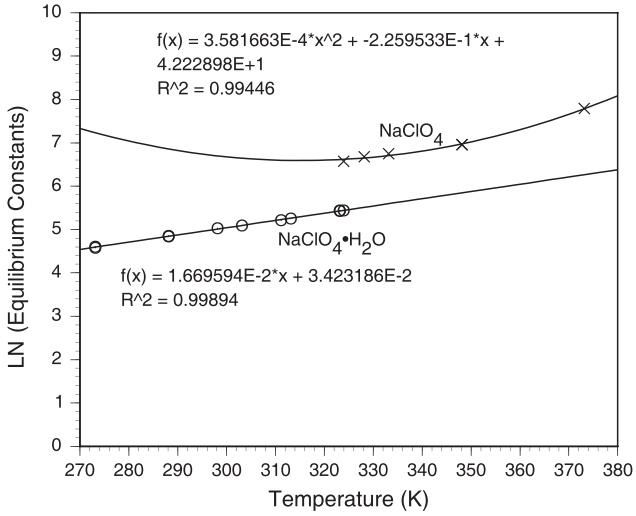

Fig. 5. The natural logarithms of the equilibrium constants for ($NaClO_4{\cdot}H_2O$) and ($NaClO_4$) over the 273–373 K temperature range (data from Linke (1965)).

taken from Ananthaswamy and Atkinson (1984). The standard error for this set of 147 data is 0.0046 $cm^3\ kg^{1/2}\ mol^{-3/2}$ (≈0.20%).

The ρ^0 and A_v parameters cover the full range for the hot spring model (0–100 °C, 1–1000 bars). Unfortunately, this is not the case for the other density/pressure parameters.

Most of the volumetric parameters ($B^v_{c,a}$ and $C^v_{c,a}$) were taken from Krumgalz et al. (2000) (Table 2). Most of these parameter sets cover highly variable temperature ranges, which will be further discussed below under Limitations. Exceptions to this generality were that we developed new volumetric parameters for H-Cl, H-SO_4, and H-HSO_4 for higher temperature ranges of 303–373 K (Table 2). This was done by using Eqs. (6) and (7) with ρ data from ICT (1928); given known parameters and solution properties from Eq. (6), it is possible to calculate V^{ex}_{mix}, which in turn, allows calculation of volumetric parameters with Eq. (7). Fig. 6 shows that our model calculations (solid lines) are reasonably good for both HCl and H_2SO_4 over the temperature range from 273–373 K in the concentration limits of 0–2 m.

Another volumetric parameter that is important is the partial molar volume at infinite dilution ($\overline{V}^0_i$) (Eq. (6)). These calculated

Table 3
Binary Pitzer-equation parameters for cations, anions, and SiO_2. Values are from Azaroual et al. (1997) for the temperature range from 25 to 300 °C[a].

Pitzer parameters	a_1	a_2	a_3	a_4	a_5	a_6	a_7	a_8
λ_{Na,SiO_2}	−4.00465e−2	−1.042719e−4	2.889422e1	1.18862e−2	−2.2210442e−1	5.994588e−8	6.396116e−1	2.192445e−1
λ_{K,SiO_2}	−1.08594e−2	1.091756e−5	1.682361e0	3.9294e−3	8.2144e−3	−6.269780e−8	4.596629e−1	1.134805e0
λ_{Mg,SiO_2}	6.237599e0	−7.228279e−3	−7.130509e2	−3.72640e−1	−3.881288e0	4.920798e−6	−8.841767e0	2.994562e1
λ_{Ca,SiO_2}	6.237599e0	−7.228279e−3	−7.130509e2	−3.72640e−1	−3.881288e0	4.920798e−6	−8.841767e0	2.994562e1
λ_{Cl,SiO_2}	0.00	0.00	0.00	0.00	0.00	0.00	0.00	0.00
λ_{HCO_3,SiO_2}	8.5131080e0	4.553030e−3	−1.363471e2	−1.613573e0	6.822994e−1	−1.913340e−6	1.901827e0	−4.134204e0
λ_{NO_3,SiO_2}	2.94769e−2	−1.394401e−4	−2.9720621e1	1.5600e−2	−1.995569e−1	−3.284336e−8	1.19537e−1	1.54574e0
λ_{SO_4,SiO_2}	4.073755e−1	3.946412e−4	−1.054513e2	−4.8974e−2	−1.248398e0	−1.047845e−6	−7.10958e−1	7.013907e0

[a] The equation for these relationships is: $f(T) = a_1 + a_2T + a_3/T + a_4\mathrm{Ln}(T) + a_5/(T - 263) + a_6T^2 + a_7/(680 - T) + a_8/(T - 227)$.

Table 4
Ternary parameters taken from Millero and Pierrot (1998).[a]

Pitzer parameters	a_1	a_2	a_3	a_4	a_5	Temperature range (K)
$\Theta_{H,Sr}$	5.91e−2			4.5e−4		273–323
$\Theta_{H,Na}$	3.416e−2			−2.09e−4		273–323
$\Theta_{H,K}$	5.0e−3			−2.275e−4		
$\Theta_{H,Mg}$	6.2e−2			3.275e−4		273–323
$\Theta_{H,Ca}$	6.12e−2			3.275e−4		273–323
$\Theta_{Na,K}$	−5.02312111e−2	1.40213141e1				273–523
$\Theta_{Na,Mg}$	7.0e−2					298–523
$\Theta_{K,Mg}$	0.00					273–523
$\Theta_{K,Ca}$	1.156e−1					273–523
Θ_{HSO_4,SO_4}	0.00					273–473
$\Theta_{Cl,OH}$	−5.0e−2			3.125e−4	−8.362e−6	
$\Psi_{Na,K,Cl}$	1.34211308e−2	−5.10212917e0				273–523
Ψ_{Na,K,SO_4}	3.48115174e−2	−8.21656777				273–523
$\Psi_{Na,Mg,Cl}$	1.99e−2	−9.51e0				298–523
Ψ_{Na,Ca,SO_4}	−1.20e−2					273–523
$\Psi_{K,Mg,Cl}$	2.586e−2	−1.427e1				273–523
$\Psi_{K,Ca,Cl}$	4.76278977e−2	−2.70770507e1				273–523
Ψ_{K,Ca,SO_4}	0.00					273–523
$\Psi_{Cl,SO_4,Na}$	−9.00e−3					273–523
$\Psi_{Cl,SO_4,K}$	−2.12481475e−1	3.75619614e1	2.84698333e−4			273–523
$\Psi_{Cl,SO_4,Ca}$	−1.80e−2					273–523
$\Psi_{H,Sr,Cl}$	5.40e−3			−2.10e−4		273–323
$\Psi_{H,Mg,Cl}$	1.0e−3			−7.325e−4		273–323
$\Psi_{H,Ca,Cl}$	8.0e−4			−7.25e−4		273–323
$\Psi_{HSO_4,SO_4,Na}$	0.00					273–473

[a] The equation for these relationships is: $f(T) = a_1 + a_2/T + a_3T + a_4(T - 298.15) + a_5(T - 298.15)^2$.

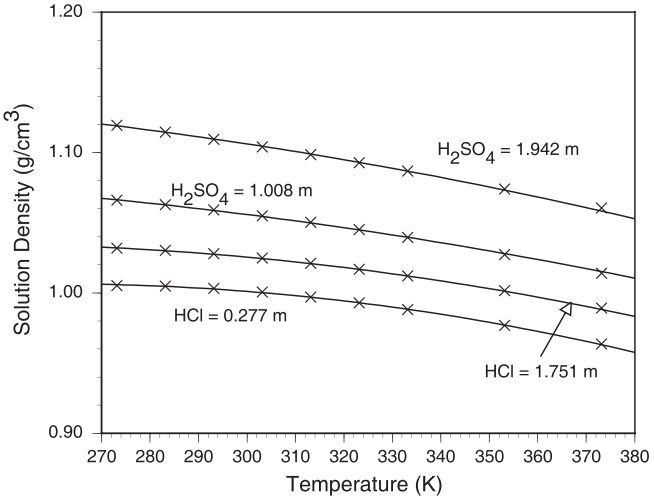

Fig. 6. The experimental (X) and model (solid line) estimates of HCl and H_2SO_4 density values between 273 and 373 K.

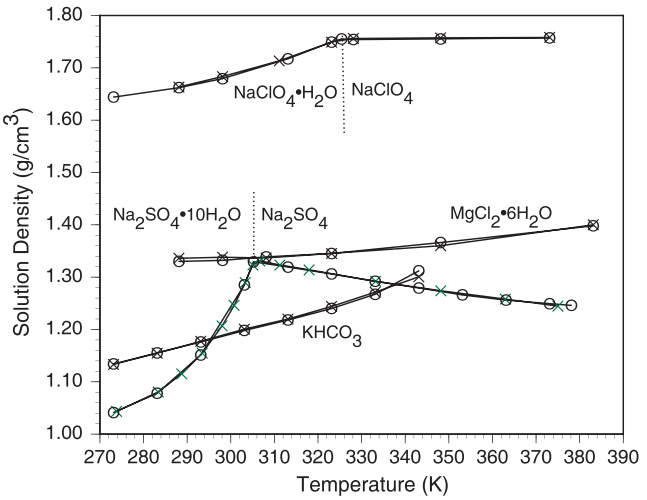

Fig. 7. The experimental (X) and model (O) estimates of density for six mineral saturated chloride, perchorate, sulfate, and bicarbonate salts.

parameters are included in Table 2. $\overline{V}^0_H = 0.0$ is an assumption made for these partial molar volumes (Millero, 1983); we also made an assumption that the $\overline{V}^0_{cl}$ that was developed from 273 to 323 K (Millero, 1983) would be valid from 273 to 373. So, it was easy to calculate the HCl values in Fig. 6 and estimate the $\overline{V}^0_c$ (cation) values in Table 2 through NaCl, KCl, $MgCl_2$, and $CaCl_2$ data (ICT,

1928; Linke, 1965). These cation ($\overline{V}_c^0$) terms were then used for calculating volumetric anions (e.g., $Na_2\underline{SO_4}$, $Na\underline{ClO_4}$, $Na_2\underline{CO_3}$, $K\underline{HCO_3}$). Mineral solubilities and densities generally increase with temperature except where solid phases change (Fig. 7). A good example is mirabilite ($Na_2SO_4{\cdot}10H_2O$) that increases rapidly in concentration at lower temperatures until it transitions to thenardite (Na_2SO_4) around 305 K, beyond which concentrations decrease with increasing temperature (Fig. 7). Overall, the model calculations are in reasonably good agreement with experimental data (Fig. 7).

In applications to Mars, we will primarily focus on hypothetical temperatures and pressures on the early surface of Mars or current Earth analogues; so little focus will deal with density and pressure parameterizations. However, subsurface processes on Mars (e.g., Clifford, 1993; Clifford and Parker, 2001; Clifford et al., 2010; Gaidos and Marion, 2003) would clearly require this density/pressure parameterization, which will be a feature of our new CHEMCHAU model.

4. Validation and limitations

Figs. 1–7 indicate the accuracy of model fits to experimental data up to some temperatures >373 K. The figures that were used as examples how we estimated equilibrium constants (Figs. 1–5) have R^2 values $\geqslant 0.994$, which is an excellent fit for establishing equilibrium constants. The % errors between the densities of experimental and model calculations in Fig. 6 range from 0.006% to 0.039%. Similarly, the % errors between densities of solutions saturated with various minerals ranged from 0.10% to 0.27%. (Fig. 7) The much higher concentrations of salts in these mineral cases (Fig. 7) is probably why the % values were much higher than the more dilute acids (Fig. 6). As a generality, the higher the solution concentrations, the larger the inaccuracies. While model fits to experimental data are encouraging and point out the self-consistency of the model and data inputs (Figs. 1–7), they are not a substitute for true validation that requires comparison to independent data for aqueous solutions. On the other hand, much of the data cited from Linke (1965) are from multiple experiments that are believed to be good estimates. Also later in Section 5, we will demonstrate a true validation between the CHEMCHAU model and independent silica data.

One of the real limitations for this CHEMCHAU code is that Pitzer parameters and equilibrium constants do not all cover the temperature range from 273 to 373 (Tables 1–4). For example, the solubility product for $KHCO_3$ only covers the temperature range from 273 to 343 (Table 1, Fig. 7). Extrapolations beyond 343 K must be done with caution. Extrapolations to temperatures <298 K (e.g., Table 3) must also be done with caution; but in this particular case from Azaroual et al. (1997), the SiO_2 parameters are changing slowly with temperature (their Fig. 2), so extrapolations to 273 K should not be a major problem. The temperature ranges given in these tables must not be confused. For example, the $Na_2SO_4{\cdot}10H_2O$ equilibrium constant given in Table 1 covers the temperature range from 273 to 306 K, and the Na_2SO_4 equilibrium constant covers the temperature range from 306 to 373 K. But this transition temperature (306 K) is not fixed within CHEMCHAU. In the presence of salts other than Na_2SO_4 (e.g., NaCl and/or $MgCl_2$), CHEMCHAU will select the solid phase that minimizes solution concentrations, which for Na_2SO_4 equilibrium could be lower or higher in temperature from the pure Na_2SO_4 phases (306 K).

5. Applications to Mars

In this section we will primarily discuss massive silica occurrences that are thought to be of hydrothermal origin, both on Mars and with Earth analogues. In the first section, we will use the theoretical foundations of the new CHEMCHAU model to characterize how amorphous silica should react to temperature and pH. In addition, we will theoretically compare silica and calcite chemistries as indicators of why martian surface chemistries are highly variable. In the second section, we will compare Earth silica analogues for Mars, both with experimental data and theoretical CHEMCHAU and FREZCHEM calculations.

5.1. Silica and carbonate chemistries

In Fig. 8 simulation, we included small amounts of $Si(OH)_4$ and $CaCO_3$, sufficiently high to lead to precipitation of silica and calcite, and 0.1 m NaCl as background composition. The solubility of silica is strongly dependent on temperature and pH. Below a pH of 7.0, silica solubility is relatively independent of pH, but still highly temperature dependent (Fig. 8). Above pH = 8.0, especially at higher temperatures, silica rises rapidly in equilibrium composition. This case is largely dependent on the reaction

$$Si(OH)_4^0 \Longleftrightarrow SiO(OH)_3^- + H^+ \tag{12}$$

where $Si(OH)_4$ activity equals $SiO(OH)_3$ activity at pH = 10.22, 9.46, and 8.91, for temperatures of 0, 50, and 100 °C, respectively. In the following section, we will discuss experimental data from natural environments and how well they correlate with theoretical models (Figs. 8–11).

We included calcite chemistry in Fig. 8 to demonstrate how highly variable T–pH chemistries could be on Mars, and why known chemistries on Mars might be vastly different from site to site. For example, Gusev Crater is where massive silica deposits are common (Crumpler et al., 2008; Ming et al., 2008; Morris et al., 2008; Rice et al., 2008; Ruff et al., 2008; Yen et al., 2008); Meridiani Planum is where acid minerals are common (Bishop et al., 2004; Klingelhöfer et al., 2004; Kargel, 2004; Kargel and Marion, 2004; Clark et al., 2005; Golden et al., 2005; Navrotsky et al., 2005; Tosca et al., 2005; Fernandez-Remolar et al., 2008; Marion et al., 2008, 2009a,b), and the Phoenix site is where perchlorates and carbonates are common (Catling et al., 2009; Fisher et al., 2008, 2009; Hecht et al., 2008, 2009a,b; Kounaves et al., 2009a,b; Boynton et al., 2009a,b; Smith et al., 2009; Marion et al., 2010a). Calcite is least soluble at high pH (low P_{CO2}) and high temperatures, which is the opposite of silica solubility that is at a maximum concentration at high pH and high temperature (Fig. 8). In this simulation calcite solubility used variable P_{CO2} concentrations (1.0e−4 to 1.0 bars) that led to pH > 6 (Fig. 8); but these

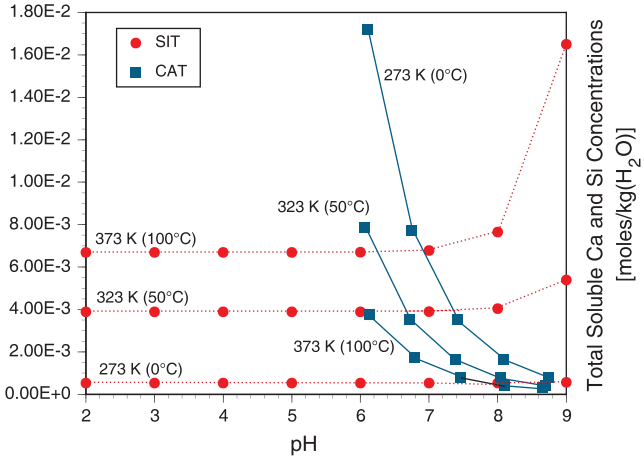

Fig. 8. The total soluble Ca (CAT) and Si (SIT) concentrations for systems in equilibrium with calcite and amorphous silica as a function of temperature and pH.

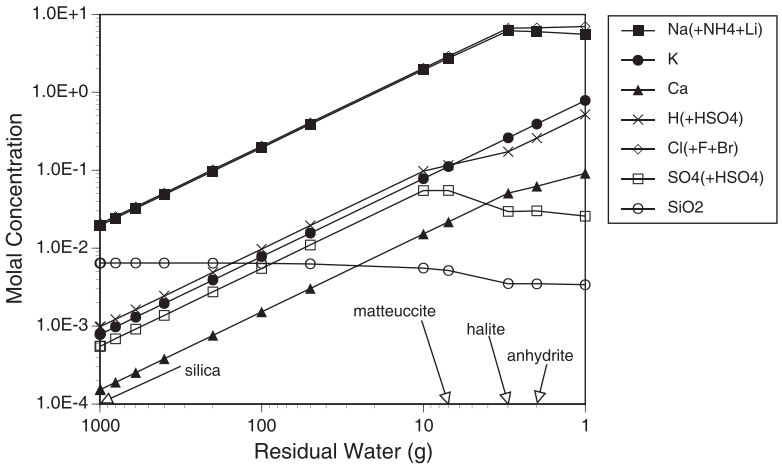

Fig. 9. Evaporation of a low pH (3.67–3.77) and high temperature (353.45 K) solution from Crystal Creek (Table 5).

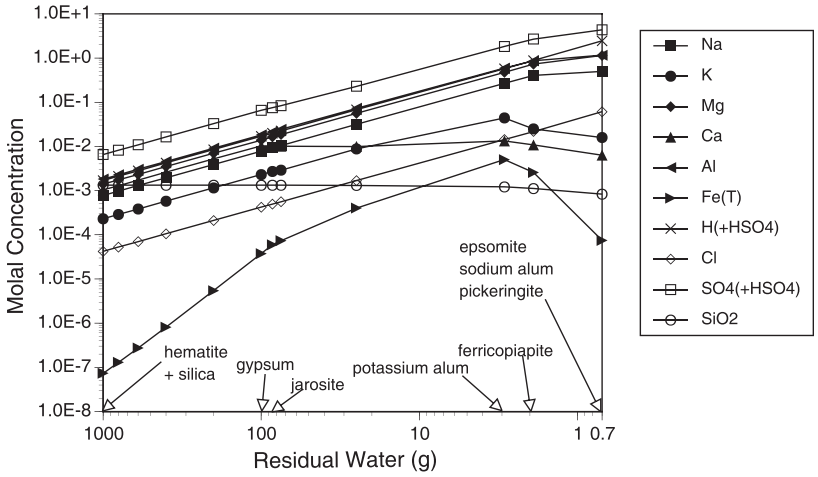

Fig. 10. Evaporation of a low pH (2.81) and low temperature (279.65 K) solution from Alluvium Creek (Table 5).

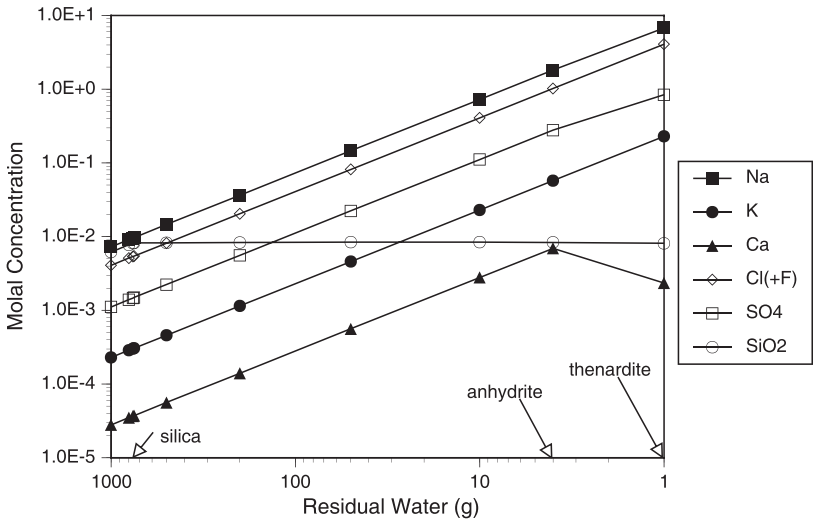

Fig. 11. Evaporation of a high pH (8.45) and high temperature (355.15 K) solution from Sodi Springs (Table 5).

assumptions are clearly not the case for silica to precipitate. In the following section, we will discuss likely environments where silica formed on Mars, which are unlikely environments for calcite formation.

We used calcite simply as an example for carbonate mineralization on Mars based on the Phoenix mission (Boynton et al., 2009a,b). But there is even more evidence for Mg carbonate formation on Mars (Bandfield et al., 2003; Ehlmann et al., 2008; Brown

et al., 2010; Morris et al., 2010) due to the prevalence of Mg salts on Mars (Clark et al., 2005; Wang et al., 2006; Zolotov and Mironenko, 2007). Magnesite, for example, is similar in solubility to calcite, being slightly more soluble at 0 °C, and slightly less soluble at 50 and 100 °C (Fig. 8). Hydromagnesite ($4MgCO_3{\cdot}Mg(OH)_2{\cdot}4H_2O$), on the other hand, is much more soluble (≈6–50-fold) than either calcite or magnesite. Also, the same case holds for silica depending on whether the precipitate is amorphous Si (Fig. 8) versus kaolinite or other clay minerals that are more insoluble than amorphous Si (Marion et al., 2009b).

5.2. Earth analogues

We choose three Earth analogues for martian silica formation that represent aqueous environments in the Yellowstone hot springs (Crystal Springs and Alluvium Creek) and Iceland (Sodi Springs) (Table 5). A potential problem with these datasets is that the concentrations were in molar units (moles/liter), while the FREZCHEM and CHEMCHAU models require molal units [moles/kg(H_2O)]. Fortunately, model-calculated molality based on the Marion (2007) approach differed from experimental molarity measurements by less than 0.3%. So, we ignored this minor factor and imported the molar data directly into the FREZCHEM and CHEMCHAU models. The values that are listed as "H" in Table 5 for Crystal Springs and Alluvium Creek were calculated based on charge balance. Model calculated pH values for Crystal Springs and Alluvium Creek using the datasets of Table 5 were 3.06 and 2.92, which are close to experimental values of 3.67–3.77 and 2.81 (Table 5). So calculating H using charge balance was a reasonable approximation.

There is evidence that suggests silica formation on Mars was significantly hydrothermal (Crumpler et al., 2008; Ming et al., 2008; Morris et al., 2008; Rice et al., 2008; Ruff et al., 2008; Yen et al., 2008). Also there are arguments that these formations were related to acid sulfate chemistry (Morris et al., 2008; McAdam et al., 2008; Ruff et al., 2008; Milliken et al., 2008; Squyres et al., 2008). The likely presence of ferric minerals with these silica deposits is also evidence of acid sulfate chemistry (Michalski et al., 2005; Squyres et al., 2008). At present, there is a limitation of CHEMCHAU because this model does not include aluminum and iron chemistries that are generally prevalent in acid sulfate systems. We ran three simulations (Table 5) that include: (1) Crystal Spring (high *T*, low pH), (2) Alluvium Creek (low *T*, low pH), and (3) Sodi Springs (high *T*, high pH). The Crystal Spring and Sodi Spring cases were high temperatures with minimal aluminum and iron chemistries that we ran with CHEMCHAU. The Alluvium Creek case was low temperature with significant aluminum and iron chemistries that we ran with FREZCHEM; this may be the most significant example of a Mars acid-sulfate analogue. At present, systems with high *T*, low pH, and significant aluminum and iron chemistries cannot be run with either FREZCHEM or CHEMCHAU.

We chose evaporation of the Crystal Creek case to represent formation of solid phases at high temperatures and low pH using CHEMCHAU. Crystal Creek is a predominantly NaCl system (Fig. 9). Silica began precipitating immediately at the initial 1000 g of water indicating that the solution was slightly supersaturated. Other salts that precipitated included matteuccite ($NaHSO_4{\cdot}H_2O$), halite (NaCl), and anhydrite ($CaSO_4$). Matteuccite typically forms in volcanic craters (http://webmineral.com), which is where Crystal Creek exists in Yellowstone hot springs.

We chose evaporation of the Alluvium Creek aqueous solution to represent the formation of solid phases likely to precipitate from acid-sulfate environments as these presumably hot aqueous solutions cooled and water evaporated. Sulfate is the dominant anion in this system (Fig. 10). This simulation was done using FREZCHEM because it deals with Fe and Al chemistries at low temperatures. According to model calculations, hematite (Fe_2O_3) and silica (SiO_2) were supersaturated at the initial concentrations (Table 5) and precipitated. Gypsum ($CaSO_4{\cdot}2H_2O$) and jarosite [$KFe_3(SO_4)_2(OH)_6$] were the next solid phases to precipitate. As the solutions evaporated, the "H" concentrations increased which caused model pH to decrease from 2.92 at water = 1000 g to 0.08 at water = 0.7 g. As a consequence, at pH = 2.11, just below where jarosite began to precipitate (Fig. 10), hematite had completely redissolved. This hematite process is reflected in the Fe concentrations in Fig. 10 that began at very low concentrations because of hematite insolubility, but rose rapidly as water was evaporated and pH dropped. The ferric minerals that precipitated at lower pH were jarosite and ferricopiapite [$Fe_5(SO_4)_6O(OH){\cdot}20H_2O$)], minerals that are common in acid-sulfate solutions (Bishop et al., 2004; Tosca et al., 2005; Marion et al., 2008). The Al minerals that precipitated were potassium alum [$KAl(SO_4)_2{\cdot}12H_2O$], sodium alum [$NaAl(SO_4)_2{\cdot}12H_2O$], and pickeringite [$MgSO_4{\cdot}Al_2(SO4)_3{\cdot}22H_2O$]. The presence of Fe minerals in these solutions are consistent with experimental data from Mars (Bishop et al., 2004; Tosca et al., 2005; Marion et al., 2008), which suggests that this Yellowstone hot spring case may be an appropriate analogue for Mars. On the other hand, in Meridiani Planum, Al is found to correlate with K but not with sulfate (Clark et al., 2005) allowing a minor but not major Al contribution to sulfate.

Silica can also precipitate at high pH values where Al and Fe are not significant and at high temperatures (355 K), which is why we chose the Sodi Springs case (Table 5) from Iceland for a simulation (Fig. 11) that was done with the CHEMCHAU model. In this case, there was a significant charge imbalance. We considered the possibility that unmeasured bicarbonate/carbonate concentrations may have existed in this system, which is similar to our assumption that H was the cause of charge imbalance for the Crystal Springs and Alluvium Creek cases in Table 5. But the necessary bicarbonate/carbonate concentrations were not consistent with a pH of 8.45 (Table 5). So we brought the system into perfect charge balance by adjusting the cation concentrations that are listed in parentheses in Table 5. Because we could not control pH through bicarbonate/carbonate chemistry at these high pH values, this simulation was run at a fixed pH = 8.45 (Table 5).

This case is a predominantly NaCl system (Fig. 11), similar to the Crystal Spring case (Fig. 9). Silica began precipitating shortly after evaporation began (Fig. 11). The only other solid phases that precipitated were anhydrite ($CaSO_4$) and thenardite (Na_2SO_4). Had this simulation been done at lower temperatures (e.g., 25 °C), then

Table 5
Experimental data that were used for simulating silica chemistries with the FREZCHEM/CHEMCHAU models.

Element	Crystal spring (m)[a]	Alluvium creek (m)[a]	Sodi spring (m)[b]
Na (+NH_4 + Li)	1.9420e−2	7.83e−4	1.0526e−2 (7.283e−3)
K	7.80e−4	2.30e−4	3.32e−4 (2.30e−4)
Mg	–	1.394e−3	–
Ca	1.52e−4	1.035e−3	3.34e−5 (2.8e−5)
Al	–	1.831e−3	–
Fe(T)	–	4.3e−5	–
H[c] (+HSO_4)	9.76e−4	1.688e−3	5.2e−9
Cl (+F + Br)	2.0384e−2	4.2e−5	4.089e−3
SO_4(+HSO_4)	5.48e−4	6.558e−3	1.114e−3
SiO_2	6.41e−3	1.628e−3	6.192e−3
pH	3.67–3.77	2.81	8.45
T (K)	353.45	279.65	355.15

[a] Nordstrom et al. (2008).
[b] Tobler et al. (2008). Concentrations in parentheses are adjusted values leading to a perfect charge balance.
[c] H concentrations for Crystal Spring and Alluvium Creek were estimated based on charge balance.

hydrated forms of these salts would have precipitated [gypsum, mirabilite ($Na_2SO_4{\cdot}10H_2O$)]. Anhydrous salts were also prevalent at the high temperature in the Crystal Creek case (Fig. 9, halite and anhydrite).

An illuminating observation regarding silica chemistry is the comparison between the experimental measurements (Table 5) and the theoretical calculations in Figs. 8–11. The measured silica concentrations are, at least, in qualitative agreement with respect to T data. For the Crystal Springs case with a temperature of 353 K, we would expect a higher silica concentration than for the Alluvium Creek case with a much lower temperature of 280 K, which agrees with the experimental data (Table 5). Similarly, raising the T to 355 K at Sodi Springs also leads to high silica concentrations (Table 5). These relative silica concentration variations are also reflected in modeling Fig. 9 (Crystal Creek, high T), Fig. 10 (Alluvium Creek, low T) and Fig. 11 (Sodi Springs, high T). Fig. 8 places equilibrium silica solubility at 354 K at 5.7e−3 m, and silica solubility at 280 K at 1.0e−3 m, which places the experimental data (Table 5) slightly supersaturated. Clearly, these silica concentrations in natural environments are near-saturation as a function of temperature. These results argue in favor of equilibrium concentrations being in close agreement with experimental silica concentrations.

6. Discussion

FREZCHEM and CHEMCHAU models were developed to cope with chemical equilibria that are a function of temperature, pressure, high concentrations, and multiple chemistries. The FREZCHEM model has a temperature range of −70 to 25 °C; the CHEMCHAU model has a temperature range of 0–100 °C. A feature of these two models is that CHEMCHAU could be used to calculate a temperature depression to 0 °C; then the resulting database at 0 °C could be used with FREZCHEM to explore these chemistries at subzero temperatures. Both models have a pressure dependence of 1–1000 bars, which has been used to explore deep ice layers (20 km) over the ocean on Europa (Marion et al., 2003b, 2005) and deep regoliths (5 km) on Mars (Gaidos and Marion, 2003). The ionic strength (I) range of these two models is 20 m using the Pitzer equations (Eqs. (1)–(3)), which is beyond other models, which use the Debye–Hückel or Davies equations that are valid to 0.1–0.5 m (PHREEQC, MINTEQ), or the Pitzer equation that is only valid to 6 m (PHRQPITZ), or models that are only valid to solution densities of 0.05–1.10 g/cm^3 (SUPCRT). The new chemistries of FREZCHEM-CHEMCHAU development in recent years have largely been selected by needs for planetary cases (e.g., Gaidos and Marion, 2003; Marion et al., 2003a,b, 2005, 2008, 2009a,b, 2010a). Other models such as PHREEQC (Parkhurst and Appelo, 1999), MINTEQ (Allison et al., 1991), PHRQPITZ (Plummer et al., 1988), and SUPCRT (Johnson et al., 1992) have broader ranges of some properties such as temperature and pressure (e.g., SUPCRT: T = 0–1000 °C, P = 1–5000 bars), but none of the latter four models can cope with I > 6 m or subzero temperatures. On the other hand, PHREEQC, PHRQPITZ, and SUPCRT have kinetic reactions that are not a component of the equilibrium FREZCHEM/CHEMCHAU models. But our two "planetary" models were ideally designed to cope with chemical equilibria across a broad range of temperatures (−70 to 100 °C), pressures (1–1000 bars), chemical compositions, and ionic strengths ($I \leqslant 20$ m) that are especially relevant to planetary applications where environments may be very different than on Earth.

7. Conclusions

The main conclusions of this study were:

(1) For the new CHEMCHAU model, Pitzer parameters, volumetric parameters, and equilibrium constants for the Na–K–Mg–Ca–H–Cl–ClO_4–SO_4–OH–HCO_3–CO_3–CO_2–O_2–CH_4–Si–H_2O system were developed that mostly covered the temperature range of 273–373 K and the pressure range of 1–1000 bars.

(2) A theoretical simulation of silica and calcite equilibrium demonstrates why surface chemistries can be vastly different on Mars due to differences in temperature and pH. Pressure, while not simulated in this paper, is an important process for subsurface chemistries on Mars.

(3) Simulation of a high temperature (353 K), low pH (3.67–3.77) (without Fe and Al chemistries) system from Yellowstone hot springs led to formation of silica along with anhydrous minerals (NaCl, $CaSO_4$) and matteuccite that typically forms in volcanic craters.

(4) Simulation of a low temperature (280 K), acid-sulfate case (low pH = 2.81) from Yellowstone hot springs led to precipitation of Fe and Al minerals along with silica, which is consistent with martian mineral assemblages.

(5) Formation of silica at high temperatures (355 K) and high pH (8.45) from an Icelandic hot springs led to precipitation of silica and anhydrous salts ($CaSO_4$, Na_2SO_4) that are clear indicators of high temperature environments.

(6) Secondary minerals associated with massive silica deposits are likely indicators of precipitation environments.

(7) Theoretical model calculations are in reasonable agreement with experimental silica concentrations, which strengthens the validity of geochemical models such as FREZCHEM and CHEMCHAU that are based on thermodynamic equilibrium.

Acknowledgments

Funding was provided by a NASA Mars Fundamental Research Project, "Martian Geochemical Applications with FREZCHEM." We thank Lisa Wable for assistance in preparing the manuscript. We thank Nicholas Tosca and an anonymous scientist for reviewing this manuscript.

References

Allison, J.D., Brown, D.S., Novo-Gradac, K.J., 1991. MINTEQA2/PRODEFA2, a geochemical assessment model for environmental systems: Version 3.0 user's manual. US Environ. Protection Agency, EPA/600/3-91/021.

Ananthaswamy, J., Atkinson, G., 1984. Thermodynamics of concentrated electrolyte mixtures. 4. Pitzer–Debye–Hückel limiting slopes for water from 0 to 100°C and from 1 atm to 1 kbar. J. Chem. Eng. Data 29, 81–87.

Azaroual, M., Fouillac, C., Matray, J.M., 1997. Solubility of silica polymorphs in electrolyte solutions, I. Activity coefficient of aqueous silica from 25 °C to 250°C, Pitzer's parameterisation. Chem. Geol. 140, 155–165.

Bandfield, J.L., Glotch, T.D., Christensen, P.R., 2003. Spectroscopic identification of carbonate minerals in the martian dust. Science 301, 1084–1087.

Bishop, J.L., Darby Dyar, M., Lane, M.D., Banfield, J.F., 2004. Spectral identification of hydrated sulfates on Mars and comparison with acidic environments on Earth. Int. J. Astrobiol. 3, 275–285.

Bishop, J.L. et al., 2009. Mineralogy of Juventae Chasma: Sulfates in the light-toned mounds, mafic minerals in the bedrock, and hydrated silica and hydroxylated ferric sulfate in the plateau. J. Geophys. Res. 114, E00D09. doi:10.1029/JE003352.

Boynton, W.V. et al., 2009a. Evidence for calcium carbonate at the Mars Phoenix landing site. Science 325, 61–64.

Boynton, W.V., Ming, D.W., Sutter, B., Arvidson, R.E., Hoffmann, J., Niles, P.B., Smith, P., and Phoenix Science Team, 2009b. Evidence for calcium carbonate at the Phoenix landing site. Lunar Planet. Sci. 40, Houston, TX. Abstract #2434.

Brown, A.J., Hook, S.J., Baldridge, A.M., Crowley, J.K., Bridges, N.T., Thomson, B.J., Marion, G.M., de Souza Filho, C.R., Bishop, J.L., 2010. Hydrothermal formation of clay-carbonate alteration assemblages in the Nili Fossae region of Mars. Earth Planet. Sci. Lett. 297, 174–182.

Carslaw, K.S., Clegg, S.L., Brimblecombe, P., 1995. A thermodynamic model of the system HCl–HNO_3–H_2SO_4–H_2O, including solubilities of HBr, from <200 to 328 K. J. Phys. Chem. 99, 11557–11574.

Catling, D.C., Claire, M.W., Quinn, R.C., Zahnle, K.J., Clark, B.C., Kounaves, S., Hecht, M.H., 2009. Possible atmospheric origins of perchlorate on Mars. Lunar Planet. Sci. 40, Houston, TX. Abstract #1567.
Christensen, P.R. et al., 2003. Morphology and composition of the surface of Mars: Mars Odyssey THEMIS results. Science 300, 2056–2061.
Clark, B.C. et al., 2005. Chemistry and mineralogy of outcrops at Meridiani Planum. Earth Planet. Sci. Lett. 240, 73–94.
Clifford, S.M., 1993. A model for the hydrologic and climatic behavior of water on Mars. J. Geophys. Res. 98, 10973–11016.
Clifford, S.M., Parker, T.J., 2001. The evolution of the martian hydrosphere: Implications for the fate of a primordial ocean and the current state of the northern plains. Icarus 154, 40–79.
Clifford, S.M., Lasue, J., Heggy, E., Boisson, J., McGovern, P.J., Max, M.D., 2010. The depth of the martian cryosphere: Revised estimates and implications for the existence and detection of subpermafrost groundwater. J. Geophys. Res. 115. doi:10.1029/2009JE003462.
Crumpler, L.S., and Athena Science Team, 2008. Geologic context of high-silica deposits on Mars from *in situ* field mapping, Columbia Hills, Gusev Crater, Mars. Lunar Planet. Sci. 39. Houston, TX. Abstract #1901.
Dobrynina, T.A., Chernyshova, A.M., Akhapkina, N.A., Rosolovskii, V.Ya., 1980. Fusion diagram of the magnesium perchlorate–water system. Russ. J. Inorg. Chem. 25, 1237–1239.
Ehlmann, B.L. et al., 2008. Orbital identification of carbonate-bearing rocks on Mars. Science 322, 1828–1832.
Fernandez-Remolar, D.C., Prieto-Ballesteros, O., Rodriguez, N., Gomez, F., Amils, R., Gomez-Elvira, J., Stoker, C., 2008. Underground habitats found in the Rio Tinto Basin: An approach to Mars subsurface life exploration. Astrobiology 8, 1023–1047.
Fisher, D.A., Hecht, M.H., Kounaves, S., Catling, D., 2008. Effects of deliquescent salts in soils of polar Mars on the flow of the Northern Ice Cap. Eos Trans. AGU (Fall Suppl.) 89 (53). Abstract U11B-0019.
Fisher, D.A., Hecht, M.H., Kounaves, S., Catling, D., 2009. Perchlorate found by Phoenix could provide a mobile brine sludge at the bed of Mars northern ice cap that would allow flow with very low basal temperatures: Possible mechanism for water table re-charge. Lunar Planet. Sci., Houston, TX. Abstract #2281.
Gaidos, E.J., Marion, G.M., 2003. Geological and geochemical legacy of a cold early Mars. J. Geophys. Res. 108. doi:10.1029/2002JE002000.
Glotch, T.D., Bandfield, J.L., Christensen, P.R., Calvin, W.M., McLennan, S.M., Clark, B.C., Rogers, A.D., Squyres, S.W., 2006. Mineralogy of the light-toned outcrop at Meridiani Planum as seen by the Miniature Thermal Emission Spectrometer and implications for its formation. J. Geophys. Res. 111. doi:10.1029/2005JE02672.
Golden, D.C., Ming, D.W., Morris, R.V., Mertzman, S.A., 2005. Laboratory-simulated acid-sulfate weathering of basaltic materials: Implications for formation of sulfates at Meridiani Planum and Gusev Crater, Mars. J. Geophys. Res. 110, E12S07. doi:10.1029/2005JE002451.
Golden, D.C., Ming, D.W., Morris, R.V., Graff, T.G., 2008. Synthetic (hydrothermal) hematite-rich Mars-analog spherules from acid-sulfate brines: Implications for formation and diagenesis of hematite spherules in outcrops at Meridiani Planum, Mars. Lunar Planet. Sci. 39, Houston, TX. Abstract #2053.
Greenberg, J.P., Moller, N., 1989. The prediction of mineral solubilities in natural waters: A chemical equilibrium model for the Na–K–Ca–Cl–SO_4–H_2O system to high concentrations from 0 to 250 °C. Geochim. Cosmochim. Acta 53, 2503–2518.
He, S., Morse, J.W., 1993. The carbonic acid system and calcite solubility in aqueous Na–K–Ca–Mg–Cl–SO_4 solutions from 0 to 90 °C. Geochim. Cosmochim. Acta 57, 3533–3554.
Hecht, M.H. et al., 2008. Discovery of perchlorate at the Phoenix landing site. Eos Trans. AGU (Fall Suppl.) 89 (53). Abstract U14A-04.
Hecht, M.H. et al., 2009a. Perchlorate in martian soil: Evidence and implications. Lunar Planet. Sci. 40, Houston, TX. Abstract #2420.
Hecht, M.H. et al., 2009b. Detection of perchlorate and the soluble chemistry of martian soil at the Phoenix lander site. Science 325, 64–67.
ICT, 1928. International Critical Tables. McGraw-Hill, New York.
Johnson, J.W., Oelkers, E.H., Helgeson, H.C., 1992. SUPCRT92: A software package for calculating the standard molal thermodynamic properties of minerals, gases, aqueous species, and reactions from 1 to 5000 bars and 0 to 1000°C. Comput. Geosci. 18, 899–947.
Kargel, J.S., 2004. Proof of water, hints of life? Science 306, 1689–1691.
Kargel, J.S., Marion, G.M., 2004. Mars as a salt-, acid-, and gas-hydrate world. Lunar Planet. Sci. 35, Houston, TX. Abstract #1965.
Kargel, J.S., Furfaro, R., Prieto-Ballesteros, O., Rodriguez, J.A.P., Montgomery, D.R., Gillespie, A.R., Marion, G.M., Wood, S.E., 2007. Martian hydrogeology sustained by thermally insulating gas and salt hydrates. Geology 35, 975–978.
Klingelhöfer, G. et al., 2004. Jarosite and hematite at Meridiani Planum from Opportunity's Mössbauer Spectrometer. Science 306, 1740–1745.
Kounaves, S.P., Catling, D., Clark, B.C., DeFlores, L., Gospodinova, K., Hecht, M.H., Kapit, J., Ming, D.W., Quinn, R.C., and Phoenix Science Team, 2009a. Aqueous carbonate chemistry of the martian soil at the Phoenix landing site. Lunar Planet. Sci. 40, Houston, TX. Abstract #2489.
Kounaves, S.P. et al., 2009b. The wet chemistry experiments on the 2007 Phoenix Mars Scout Lander Mission: Data analysis and results. J. Geophys. Res. doi:10.1029/2009JE003424.
Krumgalz, B.S., Pogorelskii, R., Sokolov, A., Pitzer, K.S., 2000. Volumetric ion interaction parameters for single-solute aqueous electrolyte solutions at various temperatures. J. Phys. Chem. Ref. Data 29, 1123–1140.
Lide, D.R. (Ed.), 1994. Handbook of Chemistry and Physics, 75th ed. CRC Press, Boca Raton, Florida.
Linke, W.F., 1958. Solubilities of Inorganic and Metal Organic Compounds, fourth ed., vol. I. Am. Chem. Soc., Washington, DC.
Linke, W.F., 1965. Solubilities of Inorganic and Metal Organic Compounds, fourth ed., vol. I. Am. Chem. Soc., Washington, DC.
Marion, G.M., 1997. A theoretical evaluation of mineral stability in Don Juan Pond, Wright Valley, Victoria Land. Antarct. Sci. 9, 92–99.
Marion, G.M., 2001. Carbonate mineral solubility at low temperatures in the Na–K–Mg–Ca–H–Cl–SO_4–OH–HCO_3–CO_3–CO_2–H_2O system. Geochim. Cosmochim. Acta 65, 1883–1896.
Marion, G.M., 2002. A molal-based model for strong acid chemistry at low temperatures (<200 to 298 K). Geochim. Cosmochim. Acta 66, 2499–2516.
Marion, G.M., 2007. Adapting molar data (without density) for molal models. Comput. Geosci. 33, 829–834.
Marion, G.M., Farren, R.E., 1999. Mineral solubilities in the Na–K–Mg–Ca–Cl–SO_4–H_2O system: A re-evaluation of the sulfate chemistry in the Spencer–Møller–Weare model. Geochim. Cosmochim. Acta 63, 1305–1318.
Marion, G.M., Kargel, J.S., 2008. Cold Aqueous Planetary Geochemistry with FREZCHEM: From Modeling to the Search for Life at the Limits. Springer, Berlin.
Marion, G.M., Catling, D.C., Kargel, J.S., 2003a. Modeling aqueous ferrous iron chemistry at low temperatures with application to Mars. Geochim. Cosmochim. Acta 67, 4251–4266.
Marion, G.M., Fritsen, C.H., Eicken, H., Payne, M.C., 2003b. The search for life on Europa: Limiting environmental factors, potential habitats, and Earth analogues. Astrobiology 3, 785–811.
Marion, G.M., Kargel, J.S., Catling, D.C., Jakubowski, S.D., 2005. Effects of pressure on aqueous chemical equilibria at subzero temperatures with applications to Europa. Geochim. Cosmochim. Acta 69, 259–274.
Marion, G.M., Catling, D.C., Kargel, J.S., 2006. Modeling gas hydrate equilibria in electrolyte solutions. CALHAD 30, 248–259.
Marion, G.M., Kargel, J.S., Catling, D.C., 2008. Modeling ferrous-ferric iron chemistry with application to martian surface geochemistry. Geochim. Cosmochim. Acta 72, 242–266.
Marion, G.M., Catling, D.C., Kargel, J.S., 2009a. Br/Cl portioning in chloride minerals in the Burns formation on Mars. Icarus 200, 436–445.
Marion, G.M., Crowley, J.K., Thomson, B.J., Kargel, J.S., Bridges, N.T., Hook, S.J., Baldridge, A., Brown, A.J., Ribeiro da Luz, B., Souza Filho, C.R., 2009b. Modeling aluminum–silicon chemistries and application to Australian acidic playa lakes as analogues for Mars. Geochim. Cosmochim. Acta 73, 3493–3511.
Marion, G.M., Catling, D.C., Zahnle, K.J., Claire, M.W., 2010a. Modeling aqueous perchlorate chemistries with applications to Mars. Icarus 207, 675–685.
Marion, G.M., Kargel, J.S., Crowley, J.K., Catling, D.C., 2010b. Modeling hydrothermal systems on Mars. Lunar Planet. Sci. 41, Houston, TX. Abstract #1393.
Marion, G.M., Mironenko, M.V., Roberts, M.W., 2010c. FREZCHEM: A geochemical model for cold aqueous solutions. Comput. Geosci. 36, 10–15.
McAdam, A.C., Zolotov, M.Yu., Mironenko, M.V., Sharp, T.G., 2008. Formation of silica by low-temperature acid alteration of Martian rocks. J. Geophys. Res. 113, doi:10.1029/2007JE003056.
McCubbin, F.M., Tosca, N.J., Smirnov, A., Nekvasil, H., Steele, A., Fries, M., Lindsley, D.H., 2009. Hydrothermal jarosite and hematite in a proxene-hosted melt inclusion in martian meteorite Miller Range (MIL) 03346; Implications for magmatic-hydrothermal fluids on Mars. Geochim. Cosmochim. Acta 73, 4907–4917.
McLennan, S.M. et al., 2005. Provenance and diagenesis of the evaporite-bearing Burns formation, Meridiani Planum, Mars. Earth Planet. Sci. Lett. 240, 95–121.
Michalski, J.R., Kraft, M.D., Sharp, T.G., Williams, L.B., Christensen, P.R., 2005. Mineralogical constraints on the high-silica martian surface component observed by TES. Icarus 174, 161–177.
Millero, F.J., 1983. Influence of pressure on chemical processes in the sea. Chem. Oceanogr. 8, 1–88 (Chapter 43).
Millero, F.J., Pierrot, D., 1998. A chemical equilibrium model for natural waters. Aquatic Chem. 4, 153–199.
Milliken, R.E. et al., 2008. Spectral evidence for sedimentary silica on Mars. Lunar Planet. Sci. 39, Houston, TX. Abstract #2025.
Ming, D.W. et al., 2008. Geochemical properties of rocks and soils in Gusev Crater, Mars: APXS results from Cumberland Ridge to Home Plate. Lunar Planet. Sci. 39, Houston, TX. Abstract #1068.
Moller, N., 1988. The prediction of mineral solubilities in natural waters: A chemical equilibrium model for the Na–Ca–Cl–SO_4–H_2O system, to high temperature and concentration. Geochim. Cosmochim. Acta 52, 821–837.
Morris, R.V., Ming, D.W., Gellert, R., Yen, A., Clark, B.C., Graff, T.G., Arvidson, R.E., Squyres, S.W., Athena and CRISM Science Teams, 2008. The hydrothermal system at Home Plate in Gusev Crater, Mars: Formation of high silica material by acid-sulfate alteration of basalt. Lunar Planet. Sci. 39, Houston, TX. Abstract #2208.
Morris, R.V. et al., 2010. Identification of carbonate-rich outcrops on Mars by the Spirit Rover. Science 329, 421–424.
Navrotsky, A., Lázár, F.F., Drouet, C., 2005. Jarosite stability on Mars. Icarus 176, 250–253.
Nordstrom, D.K., McCleskey, R.B., Ball, J.W., 2008. Sulfur geochemistry of hydrothermal waters in Yellowstone National Park: IV. Acid-sulfate waters. Appl. Geochem. doi:10/1016/j.apgeochem.2008.11.019.
Oehler, D.Z., Allen, C.C., 2008. Ancient hydrothermal springs in Arabia Terra, Mars. Lunar Planet. Sci. 39, Houston, TX. Abstract #1949.

Parkhurst, D.L., Appelo, C.A.J., 1999. User's guide to PHREEQC (Version 2) – A computer program for speciation, batch-reaction, one-dimensional transport, and inverse geochemical calculations. US Geol. Survey, Water Resources Investigations Report 99-4259.

Pestova, O.N., Myund, L.A., Khripun, M.K., Prigaro, A.V., 2005. Polythermal study of the systems $M(ClO_4)_2$–H_2O (M^{2+} = Mg^{2+}, Ca^{2+}, Sr^{2+}, Ba^{2+}). Russ. J. Appl. Chem. 78, 409–413.

Pitzer, K.S., 1991. Ion interaction approach: Theory and data correlation. In: Pitzer, K.S. (Ed.), Activity Coefficients in Electrolyte Solutions, second ed. CRC Press, Boca Raton, pp. 75–153.

Pitzer, K.S., 1995. Thermodynamics, third ed. McGraw-Hill, New York.

Plummer, L.N., Parkhurst, D.L., Fleming, G.W., Dunkle, S.A., 1988. A computer program incorporating Pitzer's equations for calculation of geochemical reactions in brines. US Geol. Survey, Water-Resources Investigation Report 88-4153.

Raju, K.U.G., Atkinson, G., 1990. The thermodynamics of "scale" mineral solubilities. 3. Calcium sulfate in aqueous NaCl. J. Chem. Eng. Data 35, 361–367.

Rice, M.S., Bell III, J.F., Wang, A., Cloutis, E.A., 2008. VIS–NIR spectral characterization of Si-rich deposits at Gusev Crater, Mars. Lunar Planet. Sci. 39, Houston, TX. Abstract #2138.

Rodgers, K.A., Cook, K.L., Browne, P.R.L., Campbell, K.A., 2002. The mineralogy, texture and significance of silica derived from alteration by steam condensate in three New Zealand geothermal fields. Clay Miner. 37, 299–322.

Ruff, S.W., Farmer, J.D., Arvidson, R.E., Squyres, S.W., Christensen, P.R., and Athena Science Team, 2008. The nature and distribution of silica at Home Plate in Gusev Crater, Mars: Evidence for a hydrothermal system. Lunar Planet. Sci. 39, Houston, TX. Abstract #2213.

Schulze-Makuch, D., Dohm, J.M., Fan, C., Fairen, A.G., Rodriguez, J.A.P., Baker, V.R., Fink, W., 2007. Exploration of hydrothermal targets on Mars. Icarus 189, 308–324.

Schwenzer, S.P., Kring, D.A., 2008. Inferred impact-generated hydrothermal mineral assemblages in basaltic regions of Mars. Lunar Planet. Sci. 39, Houston, TX. Abstract #1817.

Smith, P.H. et al., 2009. H_2O at the Phoenix landing site. Science 325, 58–61.

Spencer, R.J., Moller, N., Weare, J.H., 1990. The prediction of mineral solubilities in natural waters: A chemical equilibrium model for the Na–K–Ca–Mg–Cl–SO_4–H_2O system at temperatures below 25 °C. Geochim. Cosmochim. Acta 54, 575–590.

Squyres, S.W. et al., 2007. Pyroclastic activity at Home Plate in Gusev Crater, Mars. Science 316, 738–742.

Squyres, S.W. et al., 2008. Detection of silica-rich deposits on Mars. Science 320, 1063–1067.

Tobler, D.J., Stefansson, A., Benning, L.G., 2008. *In-situ* grown silica sinters in Icelandic geothermal areas. Geobiology 6, 481–502.

Tosca, N.J., McLennan, S.M., Lindsley, D.H., Schoonen, M.A.A., 2004. Acid-sulfate weathering of synthetic martian basalt: The acid fog model revisited. J. Geophys. Res. 109. doi:10.1029/2003JE002218.

Tosca, N.J., McLennan, S.M., Clark, B.C., Grotzinger, J.P., Hurowitz, J.A., Knoll, A.H., Schröder, C., Squyres, S.W., 2005. Geochemical modeling of evaporation processes on Mars: Insight from the sedimentary record at Meridiani Planum. Earth Planet. Sci. Lett. 240, 122–148.

Wagner, W., Pruss, A., 2002. The IAPWS formulation 1995 for the thermodynamic properties of ordinary water substance for general and scientific use. J. Phys. Chem. Ref. Data 31, 387–535.

Wang, A. et al., 2006. Sulfate deposition in subsurface regolith in Gusev Crater, Mars. J. Geophys. Res. 111, E02S17. doi:10.1029/2005JE002513.

Yen, A.S. et al., 2008. Hydrothermal processes at Gusev Crater: An evaluation of Paso Robles class soils. J. Geophys. Res. 113, E06S10. doi:10.1029/2007JE002978.

Zolotov, M.Y., Mironenko, M.V., 2007. Timing of acid weathering on Mars: A kinetic–thermodynamic assessment. J. Geophys. Res. 112, E07006. doi:10.1029/2006JE002882.